Journal of Solid Mechanics Vol. 17, No. 2 (2025) pp. 211-222
DOI: 10.60664/jsm.2025.1187309

Research Paper

A Novel Capacitive Receiver of an Ultrasonic Proximeter Enhanced by PDMS Gap

S. Kiyasatfar [1], B. Mohammadi Alasti [1], M. Fathalilou [2 *], G. Rezazadeh[2], M. Abbasgholipour [1]

[1]*Department of Mechanical Engineering of Biosystems, Bonab Branch, Islamic Azad University, Bonab, Iran*
[2]*Mechanical Engineering Department, Urmia University, Urmia, Iran*

Received 17 October 2024; Received in revised form 18 October 2025; Accepted 22 October 2025

ABSTRACT

This paper presents a novel capacitive receiver for an ultrasonic proximeter, enhanced by a displacement-dependent porous polydimethylsiloxane (PDMS) gap. The proposed design integrates a porous PDMS dielectric layer with mechanical and dielectric properties that vary with deformation, significantly improving device sensitivity. A comprehensive nonlinear mathematical model is developed to capture the coupled electrostatic, mechanical, and acoustic behaviors of the system. Analytical and numerical methods are used to investigate the dynamic response of the microplate receiver under electrostatic actuation and acoustic loading. Results demonstrate that incorporating the porous PDMS gap reduces the required actuation voltage by up to one-third compared to conventional air-gap designs and increases capacitance variation by more than sevenfold, particularly enhancing sensitivity at low acoustic pressures. The study highlights the critical role of displacement-dependent porosity in tailoring the device's electromechanical performance. These findings offer valuable insights for designing advanced MEMS ultrasonic sensors with improved efficiency and applicability in high-precision proximity sensing.

Keywords: MEMS; PDMS; Acoustic; Modeling; Sensitivity.

1 INTRODUCTION

MEASUREMANT plays an essential role in many aspects of our lives, from scientific research to manufacturing to healthcare. Measuring systems are used to measure a wide range of physical quantities,

*Corresponding author.
E-mail address: m.fathalilou@urmia.ac.ir (M. Fathalilou)

including temperature, pressure, flow rate, and electrical signals [1]. These systems assist scientists and engineers in designing and optimizing systems and products that are safe, efficient, and effective. Additionally, measuring drives innovation and enables engineers to predict and prevent issues before they occur [2]. The necessity for diverse measuring systems and sensors varies according to the specific physical quantity being gauged and the degree of accuracy required, contingent upon the specific application.

The development of a proximeter, also known as a proximity sensor, which can detect nearby objects without the need for any physical contact, is an intriguing example. A proximeter typically looks for changes in the field or return signal by emitting an electromagnetic field or acoustic waves. To meet the requirements of smooth multi-functional interactions, proximity sensors are expected to detect instantaneous and continuous activities like vibration, inertia, shear force, and normal force [3]. Because there are no mechanical parts and there is no physical contact between the proximeter and the target, proximeters can have high reliability and a long lifespan. A proximeter frequently measures changes in either an electrostatic field or an electromagnetic field to detect objects and can be classified as capacitive, magnetic, infrared, ultrasonic, or visual sensors based on the actuation mechanisms they use [4]. Among these, ultrasonic proximity sensors emit high-frequency sound waves and measure the reflection or absorption of those waves to detect the presence of an object. These sensors are commonly used in automotive applications and industrial automation [5]. Ultrasonic sensors are based on the Time-of-Flight (ToF) principle, which measures the time it takes for an acoustic wave to travel from the transmitter to the target and then bounce back to the receiver. They are thought to be very accurate down to very short distances [6-8]. They generally fall into two distinct categories: utilizing ultrasonics for proximity measurement and detection; when the first one detects an object passing within its range, it will emit a signal; by counting the time between two bursts of ultrasonic waves that are sent and received, the second one will precisely measure the distance from the object. These sensors are utilized, for instance, in self-driving vehicles [9] and smart parking solutions based on the Internet of Things (IoT) as occupancy detection sensors [10]. Their low cost, simple installation, low maintenance, high sensitivity and frequency, energy efficiency, and straightforward interface with a micro-controller or any type of controller are some of the primary reasons for their widespread use.

Ultrasonic proximeters based on MEMS (Micro-Electro-Mechanical Systems) are gaining popularity due to their high accuracy and compatibility with CMOS [11]. Even though the piezoelectric actuation mechanism is found in the majority of MEMS ultrasonic sensors, capacitive types are interesting due to their simplicity, sensitivity, accuracy, and compatibility with integrated circuits [12]. The physical element of the transmitter and receiver can be identical in these models.

One crucial factor influencing the functionality of capacitive MEMS is their sensitivity. In the context of capacitive MEMS proximeters, sensitivity refers to the capacity of the device to accurately gauge minute alterations in received ultrasound pressure. Higher sensitivity enables the proximeter to discern even the slightest movements or vibrations, rendering it well-suited for applications necessitating precise pressure detection. A number of proposed methods for enhancing the sensitivity of capacitive MEMS have been put forth in the literature, including electrode design, materials selection, and signal processing techniques [12, 13]. In addition to these, a number of further techniques based on increasing capacity can be employed. One such technique is the use of a dielectric material with a high dielectric constant to fill the gap between the electrodes [14]. Polydimethylsiloxane (PDMS) is the most used dielectric material in this regard thanks to its excellent mechanical properties and biocompatibility [14].

Recent advances in MEMS capacitive proximity and pressure sensors have focused extensively on optimizing gap-filling dielectrics to enhance sensitivity, reliability, and miniaturization. PDMS remains the most prominent material, favored for its high elasticity, chemical stability, biocompatibility, and facile processability. Numerous studies have demonstrated that introducing porosity or composite fillers into the PDMS matrix notably with carbon nanotubes, graphene, or ceramic nanoparticles can significantly increase the dielectric constant and deformability, leading to improved sensing performance. For example, Sadasivuni et al. [4] and Zulkifli et al. [15] reported enhanced sensitivity and flexibility in capacitive MEMS sensors with nanocomposite PDMS, while Valizadeh et al. [13] highlighted the critical role of material dielectricity in nonlinear micro-device response. Comparative studies have also addressed the advantages and trade-offs of alternative dielectrics such as SU-8, Parylene, and flexible ceramics, noting that PDMS-based configurations typically outperform in stretchability and ease of microfabrication, though often at the cost of lower intrinsic dielectric strength. However, most existing works either employ solid PDMS or focus on static or quasi-static conditions, and rarely account for displacement-dependent dielectric and mechanical properties arising from porosity evolution during dynamic loading. This study advances the field by directly modeling these nonlinear, displacement-coupled behaviors in porous PDMS gaps and systematically assessing their influence on MEMS capacitive receiver dynamics.

Specific methods are used to create porosity in PDMS to increase the deformability of the PDMS layer and consequently the system's sensitivity. This configuration represents one of the most effective practical methods for

enhancing the performance of MEMS sensors [12]. Recent research has increasingly recognized the potential of porous PDMS to enhance the sensitivity and performance of MEMS devices, owing to its tunable mechanical and dielectric properties through controlled porosity [16, 17]. Porous PDMS exhibits complex nonlinear elastic behavior that is often captured using hyperelastic constitutive models such as the Mooney-Rivlin and Neo-Hookean formulations, which effectively describe the large deformation mechanics of elastomeric materials with interconnected pore structures [15]. Moreover, PDMS exhibits notable viscoelastic behavior, characterized by time-dependent stress relaxation and hysteresis effects, which significantly influence its mechanical response under cyclic loading and dynamic conditions relevant to capacitive MEMS devices [14, 18, 19]. Experimental studies have demonstrated that the elastic modulus of porous PDMS decreases significantly with increasing pore volume fraction, allowing for increased deformability and sensitivity enhancement in capacitive sensors [20]. Moreover, the dielectric constant of PDMS can be modulated by embedding pores or conductive fillers, influencing the capacitive response of MEMS devices [21]. Specifically, the displacement-dependent dielectric permittivity in porous PDMS has been well-characterized through effective medium approximations, accounting for the air-filled pores and elastomer matrix contributions. The experimental results for porous PDMS with interconnected micro-pores demonstrate that when the strain is less than 0.3, the stress-strain relationship is relatively linear with a minimal hysteresis [22]. These insights have been incorporated in recent designs of capacitive MEMS to achieve superior performance through material and structural optimization. Our work builds upon these foundations by modeling the nonlinear coupled electromechanical effects induced by displacement-dependent porosity in PDMS gap fillers, expanding the understanding of their role in ultrasonic capacitive proximeters.

The enhanced capacitive receiver with displacement-dependent porous PDMS gap is particularly suited to applications in autonomous vehicles requiring high-sensitivity ultrasonic proximity sensing. The system can reliably detect acoustic pressure variations in the range of tens to hundreds of Pascals, consistent with ultrasonic wave amplitudes encountered in automotive obstacle and object detection scenarios. This sensitivity facilitates accurate distance and vibration measurement necessary for collision avoidance and navigation systems. However, realizing such devices in practice involves challenges associated with fabricating porous PDMS layers with controlled and reproducible pore sizes, ensuring homogeneity to achieve consistent dielectric and mechanical properties. Manufacturing constraints also include maintaining material stability under vehicular environmental conditions such as temperature fluctuations and mechanical vibrations. Addressing these considerations during prototyping and scale-up is essential to translate the demonstrated sensitivity enhancements into reliable, manufacturable ultrasonic sensors for practical autonomous driving applications.

This paper presents a novel model for the receiver element of a capacitive MEMS proximity sensor that exhibits enhanced sensitivity through the filling of the electrodes' gap with a porous PDMS. The vibrational equations of the system are derived taking into account the displacement-dependent properties of the PDMS. A numerical model reduction procedure based on the Galerkin method is conducted to solve the governing equation. The results illustrate the efficiency of the proposed model to increase the sensitivity of the proximeter as well as decrease in the required bias DC voltage. This model provides invaluable insights that can be leveraged to design and optimize the performance of other capacitive MEMS devices that utilize elastomeric gaps to enhance sensitivity.

2 MODEL DESCRIPTION

Fig. 1 provides a schematic representation of a capacitive proximeter. It comprises a circular vibrating microplate with fully clamped boundaries, situated at a gap distance of di from the stationary electrode. The gap distance is supposed to be filled by a porous PDMS. A bias voltage is applied between the electrodes to create the capacitance. By receiving the ultrasound pressure, the microplate vibrates on the elastic PDMS foundation, which its governing equations can be developed considering the Kirchhoff thin plate assumptions. Vibrations of the microplate results in the change in the capacitance, which is enhanced by the high dielectric constant of the PDMS.

The partial differential equation governing the vibrations of the plate, considering the pressures exerted from PDMS foundation (P_{fp}), the electrostatic pressure (P_{ep}), and the acoustic pressure (P_{ap}), as well as the nonlinear mid-plane stretching can be written as follows:

$$D\nabla^4\delta-\left(\frac{E_m t_m}{1-\nu^2}\right)\left(\frac{1}{2R_m}\int_0^1 \delta_{,r^2}\,dr\right)\nabla^2\delta+\left(\rho_m t_m+\rho_p\delta\right)\ddot{\delta}+\eta\dot{\delta}+P_{fp}-P_{ep}-P_{ap}=0 \tag{1}$$

where $D=E_m t_m^3/\ 12(1-\nu^2)$ is the flexural rigidity of the plate, E_m and ρ_m are the elastic modulus and mass density, R_m and t_m are the radius and thickness of the microplate, ρ_p is the PDMS density, and η is the equivalent damping ratio. The fully clamped boundary conditions can be written as $\delta(R_m,t)=\dfrac{\partial\delta}{\partial r}(R_m,t)=0$.

The electrostatic and PDMS pressures are directly dependent on the PDMS porosity (p). Since the pore size is supposed to be too smaller than the electromagnetic wavelength, the equivalent dielectric constant of the porous PDMS (k_{ep}) in the electrostatic pressure $P_{ep}=k_{ep}(p)\varepsilon_0 V^2/2(d_i-\delta)^2$, can be estimated using the effective medium theory [23]. Since the pore size (~1-10 μm) is orders of magnitude smaller than the ultrasonic electromagnetic wavelength (~1 mm or more), the porous PDMS layer is accurately represented as a homogenized dielectric medium. Effective medium theory is thus applicable for estimating the equivalent permittivity of the porous PDMS, enabling displacement-dependent dielectric modelling consistent with the mechanical deformation of pores [23]. On the other hand, the vibrations of the plate induce deformation of the porous PDMS, resulting in the application of a distributed pressure P_{fp}, to the plate. By considering the air-filled through-hole pores with a negligible density compared to the PDMS, the volume fraction of the porosity (ϕ_p) will decrease by decreasing the gap [13]. Consequently, the contribution of porosity in the gap medium will be displacement-dependent, as follows:

$$\phi_p(\omega)=\frac{\phi_p{}^i d_i-\delta}{d_i-\delta} \tag{2}$$

where $\phi_p^{\,i}$ denotes the initial volume fraction of the porosity. The effective displacement-dependent elastic modulus of the porous PDMS can be represented as following:

$$E_{eff}=E_p\left(1-\frac{\phi_p}{\phi_p^{(c)}}\right)=E_p\left(1-\frac{1}{\phi_p^{(c)}}\left(\frac{\phi_p{}^{(i)}d_i-\delta}{d_i-\delta}\right)\right) \tag{3}$$

where E_p is the PDMS elastic modulus and $\phi_p^{(c)}$ denotes the critical porosity, at which point E_m becomes zero. Considering Eq. (3), the PDMS foundation pressure can be written as follows:

$$P_{fp}=E_p\left(1-\frac{1}{\phi_p^{(c)}}\left(\frac{\phi_p{}^{(i)}d_i-\delta}{d_i-\delta}\right)\right)\frac{\delta}{d_i} \tag{4}$$

It should be noted that the elastic modulus of the elastomer can vary with changes in temperature, curing process, and hole size [13]. However, these factors are not the primary focus of this study. The microplate as the receiver is exposed to the return echo, resulting in an acoustic pressure, $P_{ap}=P_0\sin\omega t$ to the microplate. P_0 is the amplitude of the return pressure at the plate surface and ω is its frequency equal to the emitted sound frequency, i.e. the frequency of the vibrations of the emitter plate. Once the imposed pressures on the plate have been introduced, the Eq. (1) can be expressed in the following form:

$$D\nabla^5\delta-\frac{E_m t_m}{1-\nu^2}\left(\frac{1}{2R}\int_0^1 \delta_{,r}{}^2 dr\right)\nabla^2\delta+\left(\rho_m t_m+\rho_p\delta d_i\right)\delta_{,tt}+\eta\delta_{,t}+\frac{E_p}{d_i}\left(1-\frac{1}{\phi_p^{(c)}}\left(\frac{\phi_p{}^{(i)}d_i-\delta}{d_i-\delta}\right)\right)\delta-P_0 sin\omega t-\frac{k_{ep}\varepsilon_0 V^2}{2(d_i-\delta)^2}=0 \tag{5}$$

∇^2 and ∇^4 represent the Laplacian and bi-Laplacian operators, respectively.

A convenience analysis would be facilitated by presenting the governing equation in dimensionless form. This can be achieved by introducing new dimensionless variables for δ, r, and t using d_i, R_m, and characteristic time of the plate, respectively. So, we introduce $\lambda=\dfrac{\delta}{d_i}, \xi=\dfrac{r}{R_m}$, and $\tau=\dfrac{t}{T}$, where T is the characteristic time.

The resulting dimensionless equation is written as follows:

$$\nabla^4\lambda+\beta_1\Gamma\left(\lambda,\lambda\right)\nabla^2\lambda+\left(1+\beta_2\lambda\right)\lambda_{,tt}+\beta_3\lambda_{,t}+\beta_4\left(1-\frac{1}{\phi_p^{(c)}}\left(\frac{\phi_p^{(i)}-\lambda}{1-\lambda}\right)\right)\lambda-\beta_5\frac{V^2}{\left(1-\lambda\right)^2}=\beta_6\sin\left(\varpi t\right) \tag{6}$$

with the related boundary conditions as: $\lambda\left(1,\tau\right)=\lambda_{,r}\left(1,\tau\right)=0$, where,

$$\beta_1=-6\left(\frac{d_i}{t_m}\right)^2,\quad \beta_2=\frac{\rho_p}{\rho_m}\left(\frac{d_i}{t_m}\right),\quad \beta_3=\eta\frac{d_i}{\sqrt{\frac{\rho_m t_m R_m^4}{D}}},\quad \beta_4=\frac{R_m^4E_p^{(i)}}{Dd_i},\quad \beta_5=\frac{k_{ep}\varepsilon_0R_m^4}{2Dd_i^3},\quad \beta_6=\frac{R_m^4}{Dd_i}P_0 \tag{7}$$

It is evident that the equation can be used to predict the system's behavior under static loading by setting all time-dependent terms equal to zero in Eq. (6).

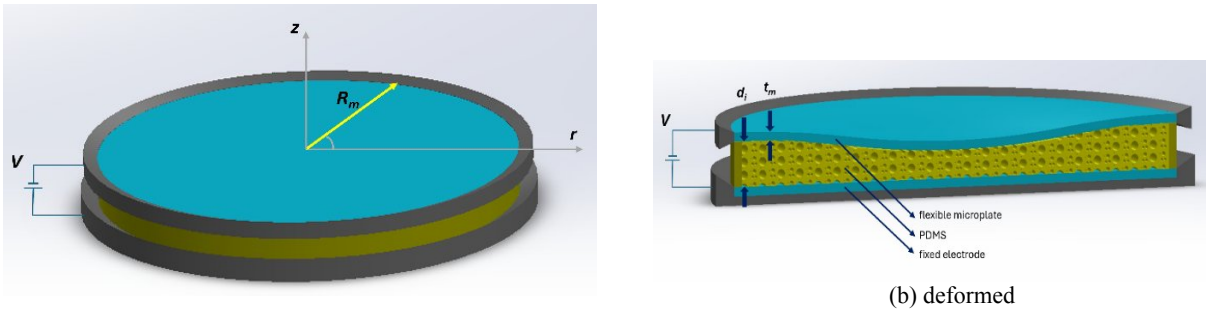

(a) undeformed

(b) deformed

Fig. 1
A schematic view of the capacitive receiver of the proximeter with porous PDMS gap.

3 SOLUTION METHODOLOGY

It is assumed that the microplate is initially deflected by a bias voltage. Consequently, the microplate experiences a deflection (λ_s) under the V_{DC} , which is then followed by the vibrational motions ($\lambda_d\left(t\right)$) under $\beta_6\sin\left(\varpi t\right)$. The static governing equation may be solved by means of the SSLM method [24]. The nonlinear terms in the governing dynamic Eq. (6) were expanded using Taylor's series, after which the resulting equation was subtracted from the static equation. The result is:

$$\begin{aligned}&\nabla^4\lambda_d+2\beta_1\Gamma\left(\lambda_s,\lambda_d\right)\nabla^2\lambda_s+\beta_1\Gamma\left(\lambda_d,\lambda_d\right)\nabla^2\lambda_s+\beta_1\Gamma\left(\lambda_s,\lambda_s\right)\nabla^2\lambda_d+2\beta_1\Gamma\left(\lambda_s,\lambda_d\right)\nabla^2\lambda_d+\beta_1\Gamma\left(\lambda_d,\lambda_d\right)\nabla^2\lambda_d+\\&\left(1+\beta_2\lambda_s\right)\lambda_{d,tt}+\beta_2\lambda_d\lambda_{d,tt}+\beta_3\lambda_{d,t}+\beta_4\left(1-\frac{1}{\phi_p^c}\left(\frac{\phi_p^{(i)}-2\lambda_s+\lambda_s^2}{\left(1-\lambda_s\right)^2}\right)\right)\lambda_d+\beta_4\left(-\frac{1}{\phi_p^{(c)}}\left(\frac{\phi_p^{(i)}-2\lambda_s+\lambda_s^2}{\left(1-\lambda_s\right)^3}\right)\right){\lambda_d}^2-\\&2\beta_5\frac{V_s^2}{\left(1-\lambda_s\right)^3}\lambda_d-3\beta_5\frac{V_s^2}{\left(1-\lambda_s\right)^4}{\lambda_d}^2=\beta_6\sin\left(\varpi t\right)\end{aligned} \tag{8}$$

The Galerkin method, utilizing basis functions from the Hilbert space, $\lambda_d\left(\xi,\tau\right)=\sum_{j=1}^{\infty}\gamma\left(\xi\right)\Lambda_j\left(\tau\right)$ is employed to transform the aforementioned equation into a reduced-order model as follows:

$$\sum_{j=1}^{\infty}\pi_{1ij}X_j(\tau)+\sum_{j=1}^{\infty}\sum_{k=1}^{\infty}\pi_{2ijk}\Lambda_j(\tau)X_k(\tau)+\sum_{j=1}^{\infty}A_{ij}\Lambda_j(\tau)+\sum_{j=1}^{\infty}B_{1ij}(\tau)\Lambda_j(\tau)+\sum_{j=1}^{\infty}\sum_{k=1}^{\infty}B_{2ijk}\Lambda_j(\tau)\Lambda_k(\tau)+$$
$$\sum_{j=1}^{\infty}\sum_{k=1}^{\infty}\sum_{l=1}^{\infty}D_{3ijkl}\Lambda_j(\tau)\Lambda_k(\tau)\Lambda_l(\tau)=f_{1i}\sin\varpi t \tag{9}$$

where,

$$\pi_{1ij}=\int_0^1\gamma_i\gamma_j(1+\beta_2\lambda_s)d\xi,\qquad \pi_{2ijk}=\int_0^1\beta_2\gamma_i\gamma_j\gamma_k d\xi,\qquad A_{ij}=\int_0^1\beta_3\gamma\gamma_j d\xi,$$
$$B_{1ij}(t)=\int_0^1\gamma_i\left(\nabla^4\gamma_j+\beta_1\Gamma(\lambda_s,\lambda)\nabla^2\gamma_j+2\beta_1\Gamma(\lambda_s,\gamma_j)\nabla^2\lambda_s+\left(\beta_4I_2+\frac{3\beta_5V_s^2}{(1-\lambda_s)^3}\right)\gamma_j\right)d\xi,$$
$$B_{2ijk}(t)=\int_0^1\gamma_i\left(2\beta_1\Gamma(\lambda_s,\gamma_j)\nabla^2\lambda_k+\beta_1\Gamma(\gamma_j,\gamma_k)\nabla^2\lambda_s-\left(\beta_4I_2+\frac{3\beta_5V_s^2}{(1-\lambda_s)^4}\right)\gamma_j\right)d\xi,$$
$$B_{3ijkl}(t)=\int_0^1\gamma_i\left(\beta_1\Gamma(\gamma_j,\gamma_k)\nabla^2\lambda_l-\frac{4\beta_5V_s^2}{(1-\lambda_s)^5}\gamma_j\gamma_k\gamma_l\right)d\xi,\qquad f_{1i}=\int_0^1\gamma_i\beta_6 d\xi, \tag{10}$$
$$I_1=1-\frac{1}{V_p^c}\left(\frac{\phi_p^{(i)}-2\lambda_s}{1-\lambda_s}+\frac{\lambda_s(\phi_p^{(i)}-\lambda_s)}{(1-\lambda_s)^2}\right),\qquad I_2=\frac{1}{\phi_p^{(c)}}\left(\frac{(\lambda_s-1)^3+(1-\lambda_s)(\lambda_s^2-2\lambda_s+\phi_p^{(i)})}{(1-\lambda_s)^4}\right)$$

Eq. (9) can be solved using an ODE solution method like the Runge-Kutta method to reach the system's time history.

4 RESULTS AND DISCUSSION

Initially, certain aspects of the given protocol are confirmed through validation with literature from previous studies. For instance, Osterberg [25] has presented empirical findings on the pull-in voltages of a silicon microplate. In a separate study conducted by Gregory and Nayfeh [26], it was demonstrated through numerical analysis that the findings of the experiment were validated by utilizing a reduced order model approach, thus further solidifying the results obtained. In air-gap capacitive microstructures, the pull-in voltage represents a critical parameter. Fig. 2 illustrates that the experimental results and the numerical findings on the estimated pull-in voltage are consistent [26]. The figure has been plotted on the basis of the material and geometrical data provided in the aforementioned research studies.

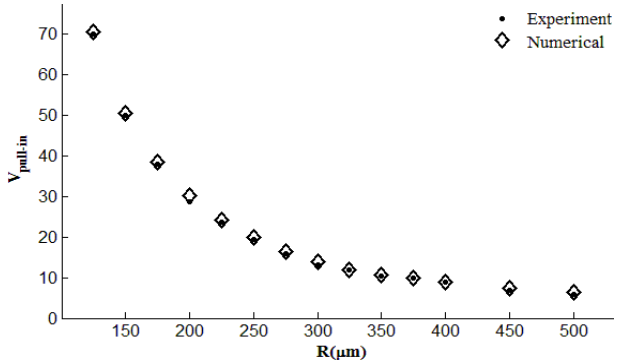

Fig.2
Variation of the pull-in voltage with the plate radios, calculated and measured experimentally [25, 26].

Moreover, for $R=150\ \mu m$, $g_0= 3\ \mu m$ and $h=6\ \mu m$, Homaei, et al. [27] have reported 73.57 V and 107.46 kHz for pull-in voltage and resonance frequency, respectively, which corroborates the obtained results. The resulting values were 73.43 V and 107.41 kHz.

Following the completion of the validation process, an investigation is now underway to ascertain the impact of the porous dielectric elastomer (DE) and its associated properties on the performance of the receiver. To this end, a system comprising the properties outlined in Table 1 and reference [25] will be subjected to analysis.

Initially, it is demonstrated that the utilization of a PDMS-gap system can influence the deflection of a microplate under identical DC voltage conditions.

Table 1
The assumed specifications of the model.

Symbols	Physical parameter	Values
E_m	Silicon elastic modulus	169 GPa
E_P	PDMS elastic modulus	69 kpa
ρ_m	Silicon density	2330 kg/m^3
ρ_P	PDMS density	965 kg/m^3
R_m	Microplate radius	150 μm
t_m	Microplate thickness	3 μm
κ_P	PDMS dielectric constant	3.448
V_p^c	Critical volume fraction of porosity	45%
ρ_a	Air density	1.293 kg/m^3
κ_a	Air dielectric constant	1
c_a	Sound velocity in air	343 m/s
ε_0	Vacuum permittivity	$8.8541878\times10^{-12}\ F/m$

Fig. 3 illustrates the variation of the ratio between the required voltage for achieving a certain static deflection with the PDMS gap configuration (V_E) and that with a conventional air-gap design (V_A) as a function of the dimensionless midpoint deflection of the microplate. The dimensionless deflection is defined as the normalized displacement at the center of the microplate divided by the initial gap thickness, providing a non-dimensional measure of deformation independent of system size. Voltage ratio values below one indicates reduced actuation voltage requirements when employing the porous PDMS gap, reflecting the enhanced electromechanical coupling achieved by the displacement-dependent dielectric properties and the compliant behavior of the PDMS foundation. It can be observed that for the given geometry and material, the ratio varies between 0.66 and 0.73. The higher dielectric constant of the gap medium in the PDMS-gap system directly increases the generated electrostatic pressure for a given voltage. Moreover, as deformation increases, the elastic pressure of the PDMS foundation also increases. This can be used to interpret the increase in the ratio, given that the rate of the electrostatic pressure in larger deflections also increases. The initial porosity volume fraction in this figure is assumed to be 0.4. This figure thereby quantifies the efficiency improvements of the proposed sensor design.

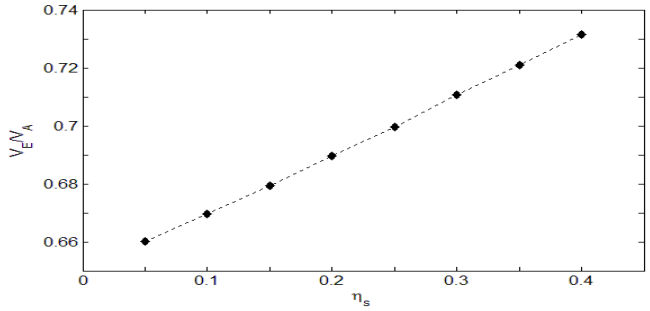

Fig.3
The ratio of the required voltage for PDMS-gap (V_E) to air-gap (V_A) versus the static deflection.

As demonstrated in the modeling section, the gap dielectric constant and elastic modulus are porosity and displacement-dependent factors in the presented model. Consequently, it is anticipated that the initial volume fraction of the porosity in the PDMS layer may influence the plate's deformation for a given voltage. Fig. 4 presents the relationship between the required voltage to achieve a specified midpoint deflection (normalized deflection of 0.4) and the initial volume fraction of porosity in the PDMS gap. As the porosity increases, the voltage needed to deform the microplate to the set deflection decreases, demonstrating the effect of enhanced compliance and reduced mechanical stiffness in the porous PDMS layer. This illustrates how adjusting the porosity parameter can be a practical design lever for lowering actuation voltage requirements and improving sensor sensitivity. This figure corroborates that by elevating the initial porosity of the elastomer to 0.45, the requisite voltage for the center point's dimensionless deformation of 0.4 can diminish by 13%.

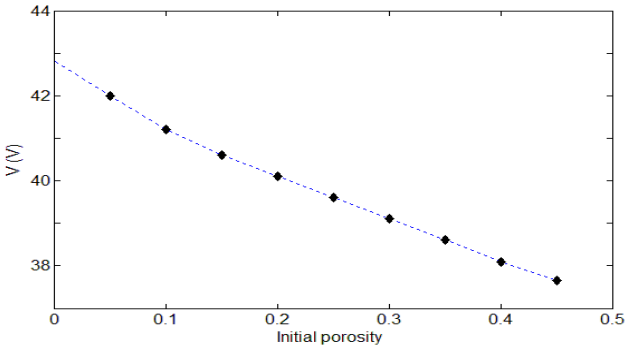

Fig.4
The required voltage for mid-point deflection of 0.4 versus porosity volume fraction.

It should be noted that while the higher dielectric constant of PDMS is of interest in reducing the required voltage and increasing sensitivity, its resistance pressure may have an inverse effect on the system's sensitivity for certain geometries of the system. This subject is illustrated in Fig. 5, which depicts the variation in the total stiffness of the system under consideration as a function of the applied DC voltage, including all the partial stiffnesses. As anticipated, the bending stiffness of the system remains constant, whereas the other three components of the system's stiffness exhibit an increase, resulting in a decrease in the total stiffness of the system. This is because the total stiffness of the system is the sum of the bending, stretching, and PDMS stiffnesses, with the electrical stiffness being subtracted from this summation. The utilization of the PDMS gap may result in either an increase in sensitivity or a decrease in sensitivity, depending on the magnitude of the increasing rate of the electrical or PDMS stiffnesses.

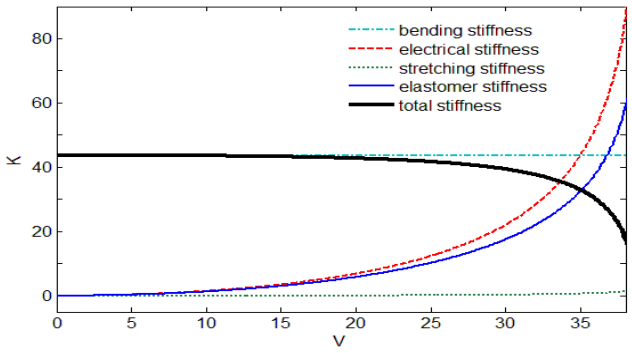

Fig.5
Variations of the system stiffnesses versus applied DC voltage for PDMS-gap configuration.

Upon the return of the transmitted acoustic wave to the microplate surface, the microplate begins to vibrate, resulting in variations of the capacitance that are proportional to the returned wave amplitude and frequency. As illustrated in Fig. 6, the utilization of a porous PDMS-gap with an initial porosity of 0.4 considerably enhances the capacitance changes by more than sevenfold, thereby markedly improving the sensitivity of the system. In this figure, a $38V$ bias voltage is considered to be applied in order to soften the system and further increase the sensitivity. The amplitude of the wave is considered to be 100 *Pa*, with the frequency being equal to the system's resonance frequency.

To quantitatively support the claim of the sevenfold increase in capacitance variation observed with the porous PDMS gap, we provide the following numerical analysis based on our modeled parameters: The capacitance change ΔC is computed as $C-C_0$, where C_0 is the baseline capacitance with no deformation, and C is the capacitance at a given acoustic pressure and deformation state, which directly is proportional to k_{ep}, ε_0 and the electrodes' surface, and inversely proportional to d_i.

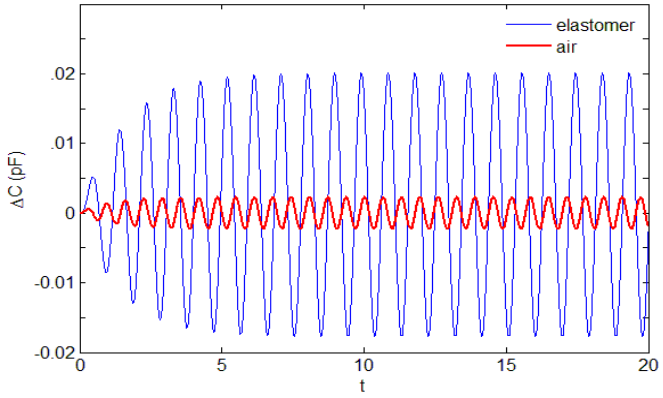

Fig.6
ΔC for V=38V and P_0=100, with and without PDMS, both on their resonance frequency.

The sensitivity of a system can be significantly influenced by the applied bias voltage, which has the effect of reducing the rigidity of the system. This phenomenon is clearly demonstrated in Fig. 7 within the context of a PDMS-gap system. This figure illustrates the dynamic response, specifically the time history of midpoint deflection, for different bias voltages at a fixed acoustic pressure (100 Pa) and dimensionless damping factor (0.1). Increasing the bias voltage leads to larger amplitude oscillations, demonstrating how the bias voltage serves as a control parameter for increasing sensor responsiveness and modulating sensitivity in the presence of the porous PDMS gap. It is observed that the magnitude of capacitance variation under identical acoustic wave pressure conditions experiences a notable increase of over threefold when the voltage level is raised from 10V to 38V.

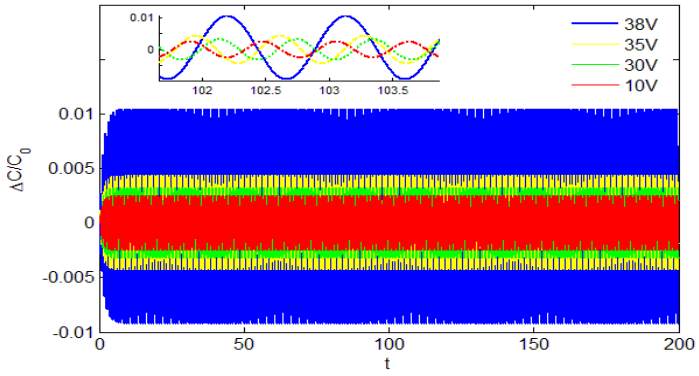

Fig.7
The time history of $\Delta C/C_0$ for different bias voltages for P=100 Pa and ζ=0.1.

The initial porosity volume fraction is another factor that can influence the sensitivity of the system. The porosity serves to reduce the elastic stiffness of the PDMS layer while maintaining the high dielectric constant of the gap medium. Fig. 8 illustrates that when the initial porosity is increased from zero to the critical volume fraction, the capacitance will change by approximately five times. This figure presents the time history of midpoint deflection for various initial porosity values of the PDMS gap at a constant acoustic pressure (100 Pa) and damping (0.1). It clearly shows that higher initial porosity leads to increased deformation amplitudes, confirming the pronounced effect of pore volume fraction on the mechanical compliance and dynamic behavior of the microplate sensor.

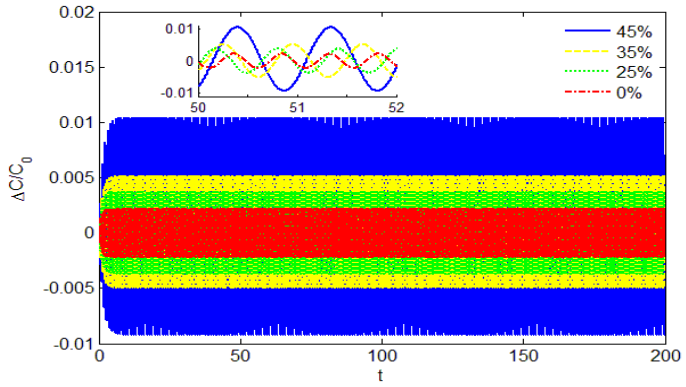

Fig.8
The time history of $\Delta C/C_0$ for different initial porosity for P=100Pa, ζ=0.1.

Fig. 9 illustrates the relationship between the variation of $\Delta C/C_0$ versus the returned pressure amplitude, comparing the PDMS and air-gap systems. The graphical representation clearly shows that in the PDMS-gap setup, as the received acoustic pressure rises, the rate of change experiences a slight decrease. This observation suggests that the sensitivity of the capacitive receiver proposed in this study is more pronounced at lower pressure levels compared to higher pressure levels. The observed reduction in sensitivity at higher acoustic pressures (Figure 9) can be attributed to the nonlinear mechanical behavior of the porous PDMS gap filler. As acoustic pressure increases, the pores within the PDMS matrix undergo progressive compression and partial collapse, leading to a saturation in deformation. This results in a nonlinear increase in the effective elastic modulus (stiffening effect) of the PDMS foundation, which acts as a stronger restoring force resisting further displacement of the microplate. Consequently, the incremental changes in capacitance diminish, reducing overall sensitivity. Additionally, as pores close under increased compression, the displacement-dependent dielectric constant of the PDMS gap approaches that of a denser solid material, limiting further modulation of the capacitance. These combined mechanical and dielectric nonlinearities explain the sensitivity drop at higher pressures and highlight the design trade-offs inherent in utilizing porous elastomeric materials for sensitivity amplification.

The data presented in Fig. 9 provides valuable insights into the behavior of the capacitive receiver under different pressure conditions, shedding light on the intricate dynamics of the PDMS-gap system. This figure confirms that the PDMS-gap device consistently achieves higher sensitivity across the range of acoustic pressures tested, particularly at lower pressures, highlighting its enhanced capability for detecting weak ultrasound signals and its suitability for high-precision proximity sensing applications.

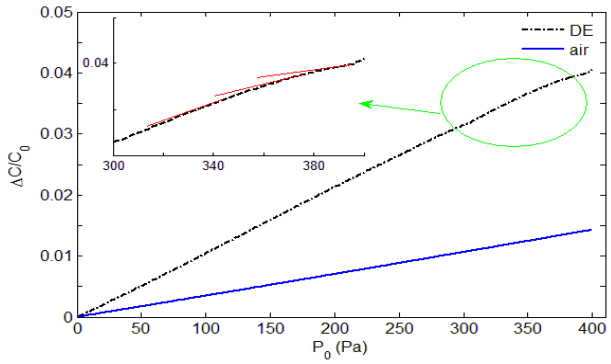

Fig.9
A comparison of the sensitivity between the air and PDMS-gap systems.

While the presented model demonstrates a significant sensitivity enhancement via the use of displacement-dependent porous PDMS as the dielectric gap filler, it is important to acknowledge several limitations intrinsic to this approach. First, the model assumes uniform pore size and distribution within the PDMS matrix, which may differ in practical fabrication scenarios, potentially affecting mechanical and dielectric uniformity. Additionally, environmental factors such as temperature variations and curing inconsistencies are not incorporated into the current

model, yet they can influence the PDMS's mechanical properties and, hence, sensor performance over time. Moreover, while our approach focuses on material-based sensitivity amplification, it is complementary to other strategies such as electrode microstructuring, signal processing enhancements, and advanced readout electronics, which address sensitivity from different perspectives. Electrode design modifications can optimize the electric field distribution and enhance capacitance variation, while signal processing techniques can improve signal-to-noise ratios and detection limits without altering the device's physical structure. Lastly, the nonlinear stiffening effect observed at higher acoustic pressures presents a trade-off: although small to moderate pressures benefit from the porous PDMS gap, sensitivity may degrade at elevated pressures, which must be considered during device design depending on the target application's operating range. These considerations point to important directions for future work, including experimental validation under varied environmental conditions and integration of complementary electrode or signal-processing optimizations.

5 CONCLUSIONS

This paper presented a novel model for the receiver of the capacitive MEMS ultrasonic proximity sensor with enhanced sensitivity. The model employs a porous PDMS material to fill the gap between the sensor's electrodes. A circular microplate was introduced as the moving electrode of the proximity sensor. A nonlinear differential equation was derived to govern the vibrational behavior of the microplate, taking into account the electrostatic, PDMS, and received acoustic pressures, as well as the mid-plane stretching of the microplate. Due to the porosity of the medium, the dielectric constant and elastic modulus of the PDMS layer were modeled as a function of the microplate displacement. Upon solving the governing equation by means of a reduced-order model, the following results were identified:

1. The utilization of the PDMS-gap can result in an increase in the deformation of the microplate for a given voltage. This phenomenon can be attributed to the higher dielectric constant of the gap medium in comparison to the air-gap system, which directly affects the magnitude of the electrostatic pressure. Nevertheless, the opposite effect of the elastic pressure of the PDMS layer may negate the outcome.
2. It has been noted that the capacitance change magnitude, when subjected to the same acoustic wave pressure conditions, exhibits a significant rise of more than three times as the voltage level is elevated from 10V to 38V. This notable enhancement in capacitance change is attributed to the softening impact induced by the bias voltage, which plays a crucial role in altering the overall behavior of the system
3. When the porosity of a material was increased from zero to the critical volume fraction, there was an observable change in the capacitance level, which can be seen to increase by a factor of about five.
4. The sensitivity of the capacitive receiver, as suggested by the current research, exhibited a greater degree of prominence when operating under lower pressure conditions as opposed to higher pressure conditions. A possible reason for this observation may be related to the increased elastic pressure generated by the PDMS layer on the microplate when exposed to elevated pressure levels. This increased elastic pressure could potentially enhance the capacitive response of the receiver, resulting in more pronounced sensitivity at lower pressure levels compared to higher pressure levels.

This study highlights the potential of porous PDMS gap fillers to substantially improve capacitive ultrasonic proximeter sensitivity; however, practical limitations related to material uniformity, environmental stability, and nonlinear pressure-dependent behavior remain. Combining this approach with other sensitivity enhancement methods such as electrode geometry optimization and advanced signal processing may yield synergistic benefits. Future work will focus on addressing these limitations experimentally and exploring integrated multi-faceted sensor improvement strategies.

REFERENCES

[1] A.H.Ghorbanpour-Arani, Wave propagation of coupled double-DWBNNTs conveying fluid-systems using different nonlocal surface piezoelasticity theories, Mechanics of Advanced Materials and Structures, 24(14),1159-1179 (2017).
[2] I. Fantozzi, S. Luozzo, M. Schiraldi, Industrial performance measurement systems coherence: A comparative analysis of current methodologies, validation and introduction to key activity indicators, Applied Sciences, 13, 235(2022).
[3] C.Tholin-Chittenden, J.F.P.J. Abascal, M. Soleimani, Automatic parameter selection of image reconstruction algorithms for planar array capacitive imaging, IEEE Sensors Journal, 18(15), 6263-6272 (2018).
[4] k.K.Sadasivuni, , Transparent and flexible cellulose nanocrystal/reduced graphene oxide film for proximity sensing, Small, 11(8), 994-1002(2015).

[5] S.D.Min, , Noncontact respiration rate measurement system using an ultrasonic proximity sensor, IEEE Sensors Journal, 10(11),1732-1739 (2010).
[6] H.K.Lee, S.I. Chang, E. Yoon, Dual-mode capacitive proximity sensor for robot application: implementation of tactile and proximity sensing capability on a single polymer platform using shared electrodes, IEEE Sensors Journal, 9(12),1748-1755 (2009).
[7] Z.Tong, An ultrasonic proximity sensing skin for robot safety control by using piezoelectric micromachined ultrasonic transducers (PMUTs), IEEE Sensors Journal, 22(18),17351-17361(2022).
[8] D.Čoko, TheraProx: capacitive proximity sensing, Electronics, 11, 393 (2022).
[9] M.Javaid, Sensors for daily life: A review,Sensors International, 2, 100121(2021).
[10] M. Khalid, From smart parking towards autonomous valet parking: A survey, challenges and future Works, Journal of Network and Computer Applications, 175, 102935 (2021).
[11] A.H. Ghorbanpour-Arani, M. Abdollahian, A. Ghorbanpour Arani, Nonlinear dynamic analysis of temperature-dependent functionally graded magnetostrictive sandwich nanobeams using different beam theories,Journal of the Brazilian Society of Mechanical Sciences and Engineering, 42(6),314 (2020).
[12] S.Valizadeh, M. Fathalilou, G. Rezazadeh, Material dielectricity effects on the performance of capacitive micro-devices: a nonlinear study, International Journal of Mechanics and Materials in Design, 19(3), 537-552(2023).
[13] S.Valizadeh, M. Fathalilou, G. Rezazadeh, Effects of the temperature-dependent behavior of the gap-filling PDMS on the response of a capacitive MEMS to the electrostatic actuation, International Journal of Applied Mechanics, 16(03),2450036 (2024).
[14] A.H. Kareem, M. Fathalilou, G. Rezazadeh, Mathematical modeling of an electrostatic MEMS with tilted elastomeric micro-pillars, Applied Mathematical Modelling, 131, 306-322 (2024).
[15] N.A.Zulkifli, Comprehensive constitutive modeling and analysis of multi-elastic polydimethylsiloxane (PDMS) for wearable device simulations, Scientific Reports, 13(1),18413 (2023).
[16] W.F.Quirós-Solano, Microfabricated tuneable and transferable porous PDMS membranes for Organs-on-Chips, Scientific Reports, 8(1),13524 (2018).
[17] M.M.Keshtiban, PDMS-based porous membrane for medical applications: design, development, and fabrication, Biomed Mater, 18(4), (2023).
[18] A.Ghorbanpour Arani, Electro-magneto wave propagation analysis of viscoelastic sandwich nanoplates considering surface effects, Proceedings of the Institution of Mechanical Engineers, Part C: Journal of Mechanical Engineering Science, 231, (2013).
[19] A.H. Ghorbanpour-Arani, Nonlocal viscoelasticity based vibration of double viscoelastic piezoelectric nanobeam systems, Meccanica, 51(1), 25-40 (2016).
[20] Z.Song, A flexible, highly sensitive porous PDMS tactile sensor based on the physical foaming method, Journal of Electronic Materials, 51(12),7173-7181(2022).
[21] M.Ghanbari, Utilizing porous dielectric material to enhance the performance of capacitive MEMS accelerometers for shaft monitoring, Measurement, 242, 115857 (2025).
[22] X.-B. Kang, W. Tan, Z.-G. Wang, Validity of effective medium theory for metal-dielectric lamellar gratings,Optics Communications, 284(19),4237-4242 (2011).
[23] Y. Zhang, The model of electric field dependent dielectric properties for porous ceramics, Journal of Applied Physics, 103(11),114103 (2008).
[24] G. Rezazadeh, M. Fathalilou, M. Sadeghi, Pull-in voltage of electrostatically-actuated microbeams in terms of lumped model pull-in voltage using novel design corrective coefficients, Sensing and Imaging: An International Journal, 12(3),117-131(2011).
[25] P.M. Osterberg, S.D. Senturia, M-TEST: A test chip for MEMS material property measurement using electrostatically actuated test structures, Journal of Microelectromechanical Systems, 6(2),107-118 (1997).
[26] G.Vogl, A. Nayfeh, A reduced-order model for electrically actuated clamped circular plates, Journal of Micromechanics and Microengineering, 15, 684 (2005).
[27] M. Homaei, Application of the electrostatic micro-speakers for producing audible directional sound, International Journal of Applied Mechanics, 12(04), 2050045(2020).